Electrically Evoked Responses in the Rabbit Cortex Induced by Current Steering With Penetrating Optic Nerve Electrodes

Yan Yan,[1] Yiliang Lu,[2] Menghui Li,[3] Zengguang Ma,[1] Pengjia Cao,[1] Yao Chen,[1] Xiaodong Sun,[4] Xinyu Chai,[1] Qiushi Ren,[3] and Liming Li[1]

[1]School of Biomedical Engineering, Shanghai Jiao Tong University, Shanghai, China
[2]Institute of Neuroscience and State Key Laboratory of Neuroscience, Shanghai Institutes for Biological Sciences, Chinese Academy of Sciences, Shanghai, China
[3]Department of Biomedical Engineering, College of Engineering, Peking University, Beijing, China
[4]Department of Ophthalmology, Shanghai First People's Hospital, School of Medicine, Shanghai Jiao Tong University, Shanghai, China

Correspondence: Liming Li, Room 517, Wenxuan Medical Building, No. 800 Dongchuan RD, Minhang District, Shanghai 200240, China; lilm@sjtu.edu.cn.

Submitted: June 23, 2015
Accepted: May 18, 2016

Citation: Yan Y, Lu Y, Li M, et al. Electrically evoked responses in the rabbit cortex induced by current steering with penetrating optic nerve electrodes. *Invest Ophthalmol Vis Sci*. 2016;57:6327–6338. DOI:10.1167/iovs.15-17543

Purpose. Current steering is a neural stimulation strategy that uses simultaneous stimulation of adjacent electrodes to produce additional intermediate stimulation sites and thus improves spatial resolution. We investigated the feasibility of current steering using electrophysiological and computational methods after implanting paired penetrating electrodes into the rabbit's optic nerve (ON).

Methods. Penetrating electrodes at different interelectrode distances were implanted into the ON and electrically evoked cortical potentials (EEPs) in V1 recorded with a 6×8 array. The current thresholds, EEP amplitudes, and spatial distributions were analyzed during current steering. Computational simulation studies were performed based on finite element models to calculate the area and spatial distribution of recruited ON fibers using a current steering stimulation strategy.

Results. Threshold reduction and EEP amplitude enhancement were found with simultaneous stimulation of closely spaced electrode pairs. Spatially shifted cortical responses were achieved using current steering, whereas the amplitudes and spatial spreads of the responses were similar to that elicited by a single electrode. Computational simulations suggested that the centroid of the ON recruitment area could be modulated by current steering while the total recruitment area did not show any appreciable variability at a fixed current intensity.

Conclusions. Current steering is a useful strategy to enhance the spatial resolution of an ON prosthesis without increasing the number of physical electrodes. This study provides useful information for optimizing the design of stimulation strategies with a penetrating ON prosthesis.

Keywords: visual prosthesis, optic nerve, electrical stimulation, current steering, electrophysiology and simulation

Visual perception provides important information about the outside world and is arguably the most relied on sense for humans; thus, its deprivation markedly affects the quality of life. Based on the development of modern biological micro-electro-mechanical systems (MEMS) and the knowledge gained from mature neural stimulation, scientists have tried to restore some degree of visual sensation by bypassing the impaired visual areas and electrically stimulating its residual functional parts.[1–8] Several research groups have been set up worldwide to address this issue, and rapid development and promising results have been achieved.[1,2,4–6,9–17] Two devices, the Argus II (Second Sight Medical Products, Sylmar, CA, USA) and Alpha IMS (Retina Implant AG, Reutlingen, Baden-Württemberg, Germany), have been clinically available in recent years. Patients using these devices regained a certain degree of visual function, such as locating and identifying objects, reading letters, and even words.[1,9,17] However, due to the limited number of stimulating electrodes, which is constrained by current engineering techniques and safety issues, the spatial resolution of present day visual prostheses is still very limited. For example, the best visual acuity measured for the Argus II trial was 20/1260[1] and 20/546 for the Alpha IMS[17]; both were within the range of "blindness" according to the World Health Organization standard (visual acuity $<$ 20/400).[18] Thus, higher acuity is still a necessary goal for artificial vision in future prostheses.

There are various types of visual prostheses, and according to the locations that are stimulated, they can be generally divided into the following categories: epiretinal,[1,3,19–22] subretinal,[2,8,13,23–25] suprachoroidal,[4,15,26,27] intrapapillary,[28] extraocular,[12] thalamic,[7] cortical,[6,10,11] and optic nerve (ON).[5,14] Among them, the ON approach may potentially achieve artificial vision over a relatively large area of the visual field. Veraat et al.[5,29] first proposed using the ON as a prosthetic target for a

blind patient and successfully implanted a cuff electrode with four surface stimulating sites. A similar method was adopted by our group to target the ON in animal experiments, but used a penetrating electrode array as the neural interface.[14,30–32] Prior studies showed that visuotopically located cortical responses could be evoked and a relatively low threshold could be achieved by penetrating ON stimulation.[31,32] However, given the small size of the ON, and the compact arrangement of retinal ganglion cell fibers, the problem of limited electrode numbers remains particularly challenging.

Similar stimulation difficulties were also encountered in other functional neural prostheses, such as cochlear implants, and current steering was introduced to address the problem.[33,34] Current steering is a subcategory of field shaping strategies that is widely used in neural stimulation. The goal of these strategies is to achieve precise control of the activated tissue region by modulating the electrical field via simultaneous stimulation of multiple electrodes. In contrast to traditional single-electrode stimulation, where only nearby neural tissue centered at the active electrode is stimulated, current steering activates neural regions that are positioned between the physical electrodes; in other words, stimulation is generated by a "virtual electrode." Previous studies have indicated that subjects with cochlear implants could hear intermediate placed perceptual pitch using current steering, and an average of four to seven intermediate pitches could be induced by manipulating the current distribution applied to two simultaneously stimulated component electrodes.[33]

Although current steering has achieved remarkable effects with cochlear implants and other neural tissue stimulation, it is still unknown whether it could be used in ON stimulation, nor how well it will perform. The effect of its application may vary widely according to different neural tissues, electrode types, and stimulus parameters. Recently, current steering has been tested to modify the activity of ganglion cells in the isolated retina, as well as in vivo suprachoroidal retinal stimulation.[35–37] In this study, we implanted fine needle-type electrodes into the rabbit ON and simultaneously stimulated the paired electrodes with a current distribution that was between the two electrodes and was varied with a steering coefficient, α. We assessed changes in the pattern of cortical activity and systematically studied the properties of the cortical response to the current steering strategy. In addition, computational models based on the same stimulating parameters were established to further investigate the effect of current steering at the level of ON fibers.

Materials and Methods

Animal Preparation and Surgical Procedures

Eight healthy adult white rabbits (Fengxian, Shanghai, China) weighing 2–2.5 kg were used. Experiments received ethical approval from Shanghai JiaoTong University, and all animal procedures were conducted in accordance with the polices in the Guide to the Care and Use of Laboratory Animals issued by the National Institutes of Health and the ARVO Statement for the Use of Animals in Ophthalmic and Vision Research.

Before anesthesia, animals received an intramuscular injection of atropine sulphate (0.03–0.04 mg/kg) and dexamethasone phosphate (1.5 mg/kg) to reduce mucous secretion and cortical edema, respectively. Anesthesia was achieved by an intravenous injection of pentobarbital sodium (Urchem Ltd., Shanghai, China) at an initial dose of 5 mg/kg and then maintained with 15 mg/kg·per hour; muscular paralysis was achieved by an intravenous injection of 10 mg/kg·per hour gallamine triethiodide (Sigma-Aldrich Co., St. Louis, MO, USA). The animal was artificially ventilated by a pulmonary pump (Matrx Model 3000; Midmark, Orchard Park, NY, USA), and

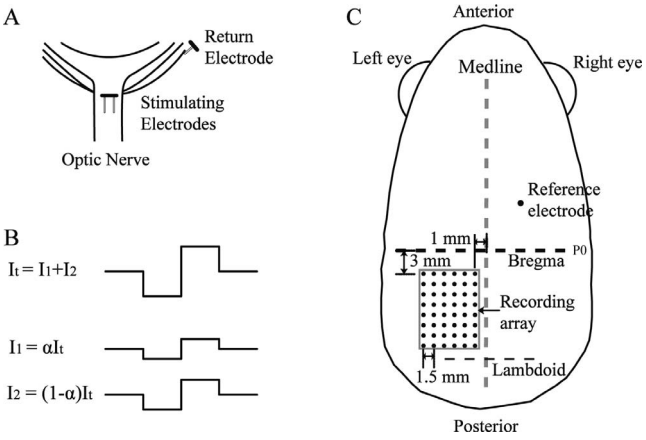

Figure 1. Schematic diagrams showing electrical stimulation of the rabbit's ON and cortical recording sites. (**A**) Stimulating electrodes were placed in the ON ~1–2 mm behind the globe. A needle-type electrode was inserted in the canthus as a return electrode. (**B**) Biphasic charge-balanced rectangular stimuli with a cathode-first phase were used for electrical stimulation. During current steering, the total current (I_t) was divided between the two electrodes with a steering coefficient α. (**C**) Cortical potentials were recorded by a 6 × 8 silver-ball electrode array (center-to-center spacing, 1.5 mm) placed epidurally over the primary visual cortex (V1).

body temperature was maintained by a feedback heating pad (Model H-KWDY-III; Xinxiaoyuan Biotech Ltd., Nanjing, China) beneath the abdomen. Rabbits were placed in a stereotaxic instrument (SN-3N; Narishige, Tokyo, Japan) to achieve stable electrophysiological recordings. The rectal temperature was maintained at ~38°C, the end-expiratory CO_2 was maintained at 4%, and the electrocardiogram was continuously monitored throughout the experiment.

The ON of the right eye was used for microelectrical stimulation, and the primary visual cortex (V1) contralateral to the stimulated ON was used for electrophysiological recordings (Fig. 1). A craniotomy extending from 1 to 9 mm lateral to the midline and from 3 to 14 mm posterior to the bregma suture was performed to expose the majority of the rabbit's V1.[38] Epidural cortical responses to ON stimulation were recorded using a custom-made 6 × 8 silver-ball electrode array. The array had a center-to-center spacing of 1.5 mm, and each silver ball was 0.3–0.4 mm in diameter with an impedance of 500–800 Ω. The visuotopic map in the rabbit V1 in relation to the recording array has been shown previously in figure 3 of Yan et al.[39] A steel screw electrode inserted into the frontal bone ipsilateral to the stimulated ON served as a reference electrode for recording, and a stainless needle electrode was inserted into the tip of ear as the ground.

The ON was exposed by making an incision ~3 mm above the upper eyelid, and blunt dissection was used to separate the orbicularis oculi and levator muscles, and the cartilage of the upper orbit was then exposed. Another incision was made between the cartilage and the frontal bone and then enlarged along its bony edge (14 mm) so that a periorbital approach could be achieved. The posterior part of the eyeball and a 3–4 mm length of the intraorbital ON were clearly visible after cutting and retraction of the superior rectus and removal of the fatty tissue around the ON.

Electrophysiological Recordings

V1 electrically evoked potentials (EEPs) in response to ON stimulation were recorded using a neurophysiology workstation (RX7; Tucker-Davis Technologies, Alachua, FL, USA) at a 6-

kHz sampling rate per channel, amplified, and band-pass filtered at 3–1000 Hz. Consecutive EEP responses were averaged ($n = 50$) and then analyzed.

The amplitude of the first major positive peak (P1) of the averaged EEP (measured as the difference between the P1 and the baseline) was used to represent EEP amplitude and the strength of the response. The channel with the highest amplitude (HCh) among the 48 recording channels was used to represent the amplitude of the array and subsequent threshold calculation. The EEP threshold was defined as the current intensity eliciting a P1 that was approximately two times the root mean square (RMS) of the baseline fluctuation.

Electrical Stimulation

Polymer-insulted platinum-iridium electrodes (PI20030.1H3, 51 mm long and 81-μm shaft diameter; Micro Probe, Inc., Gaithersburg, MD, USA) were used for ON stimulation. The electrode had an exposed 32-μm-long cone-shaped tip 12 μm in diameter; thus, the calculated exposed area was $\sim 6.14 \times 10^{-6}$ cm^2. The impedance of each electrode was 100 kΩ, measured with a 1-kHz, 100-nA sinusoidal current (impedance meter: model IMP-2MC; Micro Probe, Inc.). A stereotaxic micromanipulator (SM-11; Narishige) was used to implant electrode pairs into the ON ~1–2 mm behind the eyeball at three interelectrode distances: 200, 400, and 600 μm. The electrode pairs were inserted perpendicular to the ON fiber orientation and with a temporal-nasal (medial-lateral) arrangement (Fig. 1A). Stimulating current pulses were generated by an isolated and programmable current-source stimulator (MS16; Tucker-Davis Technologies). Biphasic charge-balanced rectangular cathodic-first current pluses were used with a phase duration of 0.5 ms, an interphase gap of 0, and at a frequency of 1 Hz. All stimuli were monopolar and used a remote stainless steel electrode placed at the canthus as the return electrode.

Single-electrode and current steering stimulation modes were systematically applied to the electrode pairs. In the single-electrode mode, only one electrode from the component pair (i.e., electrode 1 [E1] or E2) was stimulated; E1 and E2 were stimulated simultaneously in the current steering mode, wherein the current distribution between E1 and E2 was determined by the steering coefficient, α, which was defined as a fraction of the total current delivered through E1. The total current applied through the pair was I_t; therefore, the current applied to E1 is $I_1 = I_t \times \alpha$, whereas the current applied to E2 is $I_2 = I_t \times (1 - \alpha)$. Thus, $\alpha = 0$ indicates the stimulation of only E2, and $\alpha = 1$ indicates the stimulation of only E1. The current threshold for E1 (Thr_1) and E2 (Thr_2) in each pair was tested separately. The current steering base strength level I_b was set as $I_b = Thr_1 + Thr_2$; four current strength levels, $0.5I_b$, $0.75I_b$, $1I_b$, and $1.5I_b$, were studied. To explore the cortical response characteristics to current steering, a typical coefficient where $\alpha = 0.5$ was used and the EEP responses were compared with that evoked by the single-electrode mode. The coefficient α was then gradually changed in 0.1 steps to investigate the effect of the current distributions on the EEP responses.

Statistical Analysis

The spatial distribution of the cortical responses was mapped by plotting the 48 channel EEP amplitudes from the recording array. To further quantitatively analyze the spatial characteristics of EEPs evoked by certain stimuli, the EEP distribution map was fitted by a standard two-dimensional (2D) Gaussian function to determine the maximum response location (MRL) relative to the recording array. The 2D Gaussian function is

$$f(x,y) = A \exp\left(-\left(\frac{(x-x_0)^2}{2\sigma_x^2} + \frac{(y-y_0)^2}{2\sigma_y^2}\right)\right) \quad (1)$$

where the coefficient A is the amplitude, (x_0, y_0) is the center, and σ_x, σ_y are the x and y spreads of the blob. σ_x and σ_y were set to be equal, thus producing an isotropic Gaussian function. The half-width at half-maximum (HWHM) of the function curve was used to represent the extent of the spatial spread of the cortical responses.

The results are shown as the mean and SD, and paired data were compared with paired *t*-tests and a Student *t*-test for the other data. Comparisons were considered statistically significant when $P \leq 0.05$ for both tests.

Computational Simulation of Current Steering by Paired Electrode Stimulation

Simulation models were established using a method that was elaborated in a previous study by our group; for details, see Li et al.[40] In brief, finite-element models were established in the COMSOL Multiphysics modeling environment to compute the 3D electric potential distribution generated by stimulation using current steering. The calculated potentials were then used as data in multicompartment cable models that were constructed using NEURON software; the models used 10,000 ON fibers to predict response patterns under specific electrical stimulus conditions. The shape and parameters of the stimulating electrodes used in the simulation were the same as those used in the above electrophysiology studies. The two indices, recruitment area (RA) and shifting rate (SR), were derived from the ON fiber ensemble response pattern and used to measure the activities of the ON fibers with current steering. RA refers to the size of the region within which the ON fibers could be excited with a probability larger than 50%, SR was calculated to quantify the position of the recruitment centroid relative to the electrodes and thus was used to evaluate the degree of current steering. SR was explicitly defined as the ratio of the centroid shift from the midpoint between the two electrodes against 50% of the interelectrode distance. The values of RA and SR for a total of $5 \times 3 \times 4$ cases were calculated: α was varied from 0.1 to 0.5 in steps of 0.1, with interelectrode distances of 200, 400, and 600 μm, and stimulated by total current strength of $I_t = 0.5I_b$, $0.75I_b$, $1I_b$, and $1.5I_b$, respectively. Here we stipulate that $I_b = 14.0$ μA, an average value of the base strength levels measured in animal experiments.

Results

Electrically Evoked Cortical Potentials Response to Single-Electrode Stimulation

Stable EEPs could be recorded from the contralateral V1 following electrical stimulation of the ON. The current threshold was 6.8 ± 3.0 μA with a phase duration of 0.5 ms at 1 Hz and was equal to a charge of 3.4 ± 1.5 nC per phase ($n = 28$ in eight rabbits). Given the exposed area of the electrode tip, the charge density threshold was 553.7 ± 244.2 $\mu C/cm^2$. Figure 2 shows examples of EEP waveforms evoked by ON stimulation and a typical EEP waveform contains a major positive peak (P1) followed by a large negative peak (N1). The implicit time for the P1 was 11.0 ± 1.2 ms measured at two times threshold current ($n = 28$ in eight rabbits). The EEP amplitudes varied among the 48 cortical channels (Fig. 2B), and this is clearly demonstrated by the spatial distribution of the cortical responses shown in the color-coded map of the P1

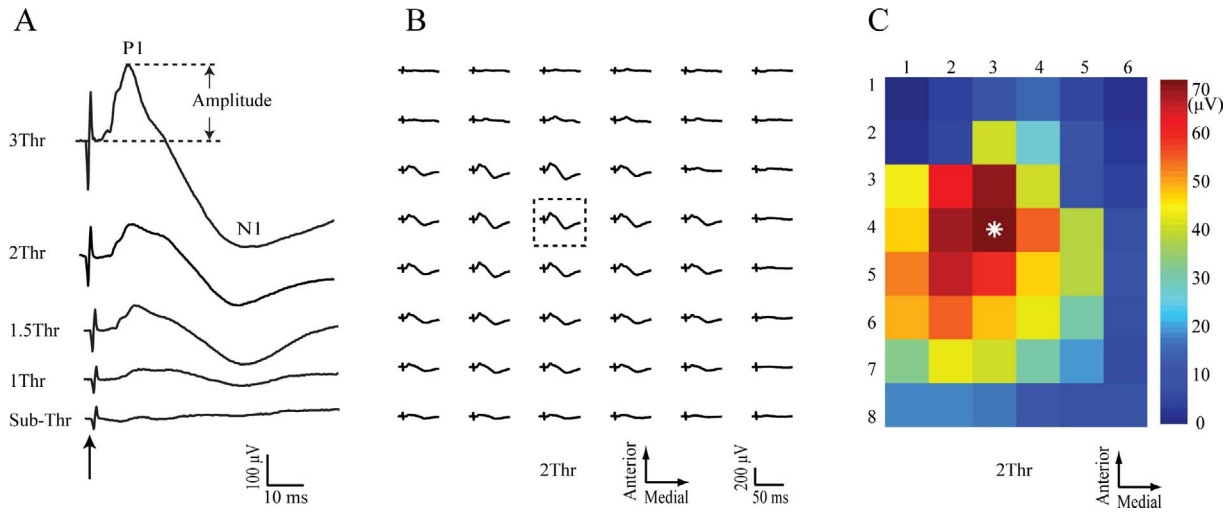

Figure 2. Typical EEPs elicited by a single electrode in the ON. (**A**) Typical EEP waveforms elicited by different current strengths ranging from sub-threshold (sub-Thr, 4 μA) to three times threshold (3Thr; 1Thr = 5 μA). The *arrow* indicates stimulus onset. All EEPs are from the channel with the highest P1 amplitude (i.e., HCh of the recording array), which is indicated by *dashed box* in **B** and *asterisk* in **C**. (**B**) Spatial distribution of EEPs recorded from the 6 × 8 array (2Thr). (**C**) The P1 amplitude values derived from **B** were plotted as a pseudo-color map.

amplitude recorded at each channel (Fig. 2C). Increasing the current strength caused an increase in the EEP amplitude, as shown in Figures 2A and 3A. The spatial spread of the response across the V1, calculated by the HWHM of the Gaussian fitting, also increased as the stimulation current increased (Figs. 3B, 3C).

Threshold and Amplitude of EEPs to Steering Stimulation

A steering coefficient of $\alpha = 0.5$ was used to investigate EEP thresholds to current steering stimulation; that is, the current is evenly distributed between the two component electrodes. Threshold reduction was seen for simultaneous stimulation of electrodes pairs, such that EEPs were evoked with current strengths that were lower than the threshold of either electrode on its own. Although we did not measure the exact threshold current for current steering, the threshold reduction could be observed qualitatively from the minimum tested current levels. Examples are shown in Figures 4A and 5C through 5E from rabbit 03. The interelectrode distance of this pair was 200 μm, and the thresholds for E1 and E2 were 7 and 5 μA, respectively. In current steering mode, cortical EEPs could be evoked with a stimulating current of $0.5I_b = 6$ μA at an α of 0.5; that is, $0.5 \times (\text{Thr}_1 + \text{Thr}_2)$ with simultaneous stimulation of E1 with 3 μA (i.e., $0.5 \times [\text{Thr}_1 + \text{Thr}_2] \times \alpha$; $0.5 \times [7 + 5] \times 0.5$); note E1 and E2 were both below their single-electrode thresholds. Four current levels, $0.5I_b$, $0.75I_b$, $1I_b$, and $1.5I_b$, were used to test EEPs responses to current steering, and the detailed current levels that could evoke EEPs for different electrode pairs are shown in Figures 4B through 4D after the currents applied to E1 or E2 were normalized according to their single-electrode thresholds. Statistical analysis of the minimum currents is shown in Figure 4E. In 87.5% of experiments with electrode pairs separated by 200 μm (7 of 8) and 100% of experiments with electrodes separated by 400 μm (4 of 4), the threshold in the steering mode was lower than the threshold of either electrode alone ($P < 0.05$); however, electrodes separated by 600 μm only produced EEPs when the current applied to one of the electrodes was at or above that electrode's threshold ($P > 0.05$).

Figure 5 shows an example of the spatial distribution of the cortical responses for electrodes 200 μm apart and stimulated at $0.5I_b$, $0.75I_b$, $1I_b$, and $1.5I_b$ current levels in the single-electrode versus current steering modes with an $\alpha = 0.5$ (rabbit 03). Different spatially distributed cortical responses could be

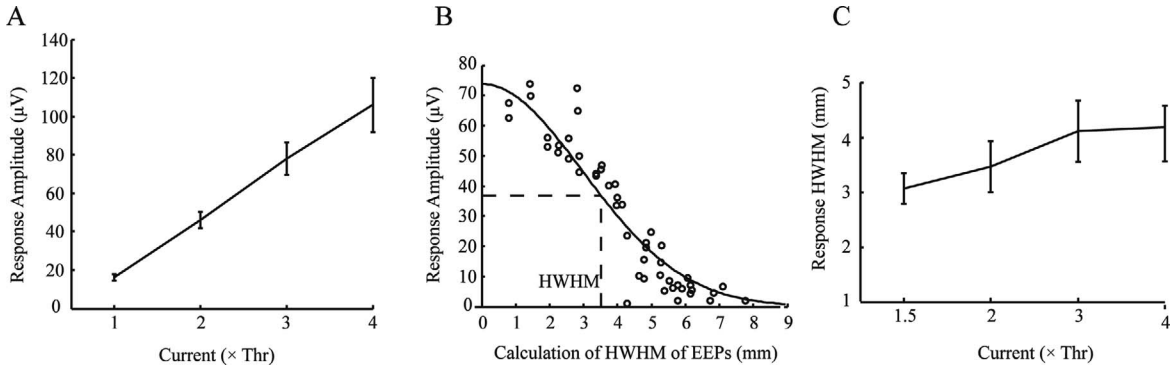

Figure 3. Plots of the amplitude and spatial spread of the cortical EEPs to ON stimulation by a single electrode and variable current strength. (**A**) Strength–amplitude relationship. (**B**) An example of the spatial spread of EEPs in response to 2Thr stimulus to illustrate the Gaussian fit calculation method for HWHM, which was used to represent the spatial spread of the cortical responses (from one single electrode). (**C**) Strength–HWHM relationships from the same animals and recordings used in **A**. Mean ± SD, $n = 28$ single electrodes in eight rabbits.

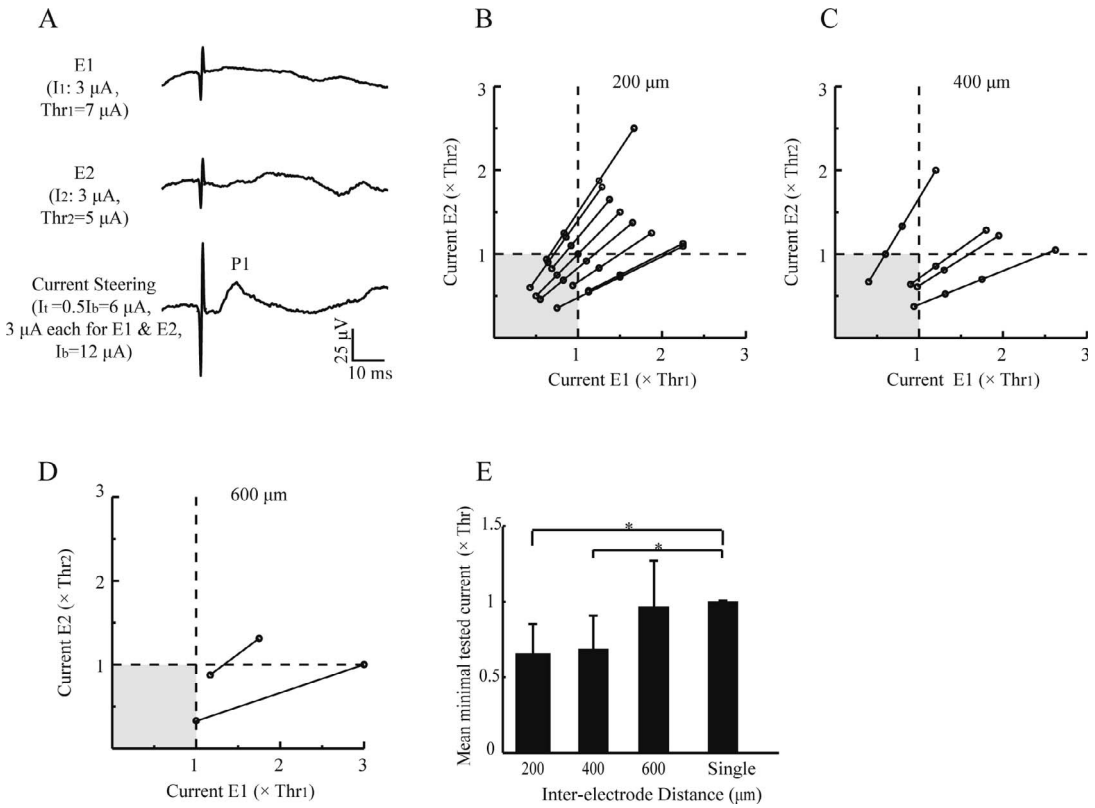

Figure 4. The minimum tested current level needed to evoke EEPs using current steering at different interelectrode distances and at an $\alpha = 0.5$. (**A**) An example of EEPs evoked at the HCh by current steering and when using below-threshold currents at each single component electrode (interelectrode distance = 200 μm, $I_t = 0.5I_b$, $\alpha = 0.5$). (**B–D**) Normalized current levels applied to electrode E1 or E2 that evoked EEPs at different interelectrode distances. Each *line* represents a different electrode pair. The *shaded area* represents below-threshold currents for both electrodes. (**E**) Average minimum tested current needed to evoke an EEP at 200 ($n = 16$ electrodes), 400 μm ($n = 8$), 600 ($n = 4$), and single electrodes ($n = 28$). $^*P < 0.05$.

evoked by separately stimulating electrode E1 (Figs. 5A, 5C) or E2 (Figs. 5B, 5E). Current steering of E1 and E2 (Fig. 5D) resulted in spatially different cortical responses in which the HChs were intermediate between those evoked by E1 or E2 alone. The spatial distribution information for current steering is statistically analyzed later in the following section.

Consistent with threshold reduction, the EEP amplitudes were higher with current steering compared to single-electrode modes with the same current. The example in Figure 5 shows that current steering of E1 and E2 with 18 μA, i.e. 9 μA at each electrode ($1.5I_b$ current level, panel d), evoked EEPs with higher amplitudes vs. stimulating either E1 or E2 with 9 μA. Further analysis showed that it was also higher than the summation of the HCh amplitudes for E1 and E2. Figure 6 shows the EEP amplitudes during current steering versus single-electrode stimulation at a $1.5I_b$ current level and with different interelectrode distances. The EEP amplitudes with current steering (current strength: I_t) at interelectrode distances of 200 and 400 μm were significantly larger than the summation of the independent EEP amplitudes evoked by single-electrode stimulation at E1 and E2 ($I_t/2$ each) ($P < 0.05$; Fig. 6); there was no amplitude enhancement with an interelectrode distance of 600 μm (Fig. 6).

Responses to Steering Stimulation While Varying the α Coefficient

Figure 7 shows three examples of cortical responses to simultaneous stimulation of a pair of electrodes, 200 μm (rabbit 03, the same data shown in Fig. 5), 400 μm (rabbit 06), and 600 μm apart (rabbit 08), as α was varied from 0 to 1 in 0.1 steps. When the current distribution between the two electrodes changed, the EEP response distribution showed a gradual spatial shift representative of a shift in the ON stimulation from one electrode to the other. A 2D Gaussian fit was used to determine the cortical activity MRLs of the EEPs evoked by the component electrodes at the various α values for quantitative analysis of the spatial shifts (see Materials and Methods). To normalize the data between different electrode pairs, as shown in Figure 8, the MRL corresponding to stimulation with $\alpha = 0$ was set as the original location for each pair, and the distance between MRLs in response to stimulation at $\alpha = 1$ versus $\alpha = 0$ was set as 1. Therefore, the cortical shifts from stimulation of $\alpha = 0.1 \sim 0.9$ were defined as the difference of their MRLs compared with $\alpha = 0$ and normalized by the MRL distance of between $\alpha = 0$ and $\alpha = 1$. Regression lines were fitted to the data and showed that there was a significant linear correlation between the various α values and the cortical MRL shifts at all the three interelectrode distances (Figs. 8A–8C: 200 μm: $r = 0.90$, $P < 0.01$, $n = 8$ in five rabbits; 400 μm: $r = 0.86$, $P < 0.01$, $n = 4$ in two rabbits; 600 μm: $r = 0.93$, $P < 0.01$, $n = 2$ in one rabbit).

Given that there is a linear relationship between the cortical shifts in the steering mode ($\alpha = 0.1 \sim 0.9$) versus the single-electrode mode ($\alpha = 0$ or 1) for all electrodes, the cortical shifts of both modes were plotted together to determine any quantitative relationship to shifts in the site of stimulation within the ON (Fig. 8D). A virtual position for the site of stimulation within the ON during the steering mode with an α coefficient was calculated as α ×

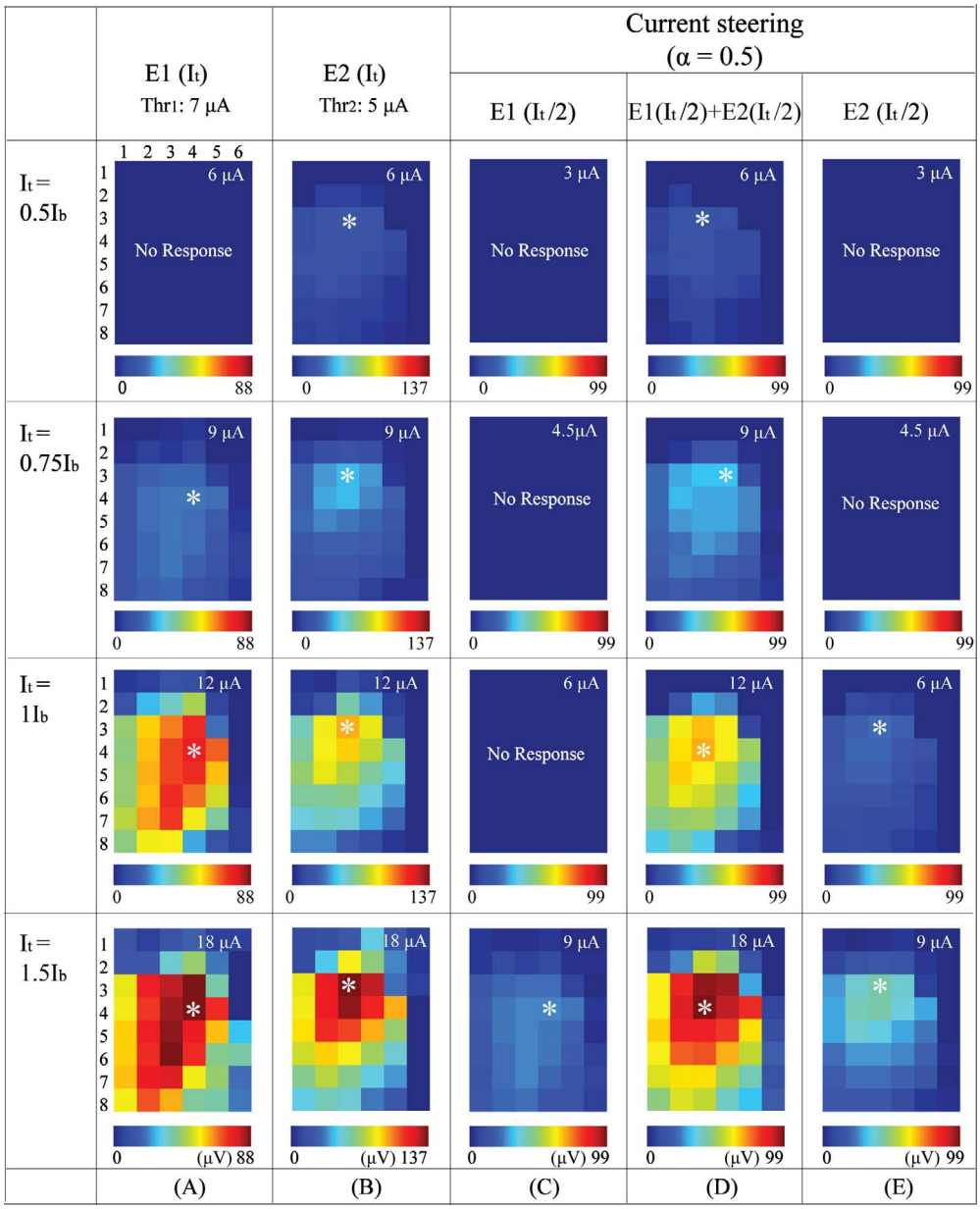

Figure 5. Spatial distribution maps comparing single-electrode versus current steering stimulation at different current strengths (interelectrode distance = 200 μm, α = 0.5). Single-electrode stimulation at E1 (**A**) or E2 (**B**) was increased in steps equal to the four total steering mode current levels: 6 (0.5I_b), 9 (0.75I_b), 12 (1I_b), and 18 μA (1.5I_b). (**C**, **E**) Single-electrode stimulation at half the steering current stimulation can be compared with the result after combing stimuli in the steering mode (**D**) at α = 0.5. *Asterisks* indicate the HChs. Data from rabbit 03.

interelectrode distance,[37] for example, α = 0 and a 600-μm interelectrode distance in ON shifts the stimulation site 0 μm, whereas an α = 0.5 shifts the stimulus point 300 μm within the ON and produces a corresponding shift in the location of the maximal cortical response. The mean MRL shift for a 600-μm ON separation was 4.44 ± 0.92 mm (n = 2 in one rabbit); for a 400-μm separation, this was 3.40 ± 1.46 mm (n = 4 in two rabbits), and for 200 μm, this was 2.16 ± 1.01 mm (n = 12 in seven rabbits, including stimulation of 400-μm pairs with an α of 0.5). A virtual minimum ON shift in the site of stimulation by 20 μm, using a step of 0.1 and electrode pairs separated by 200 μm, produced a cortical shift of 0.28 ± 0.17 mm (n = 8 in five rabbits). The average cortical magnification factor in the rabbit's V1 is approximately 0.125 mm/deg[38]; thus, the calculated shift in visual angle corresponds to 35.5 ± 7.4°, 27.2 ± 11.7°, and 17.3 ± 8.1° by, respectively, shifting the site of ON stimulation by 600, 400, and 200 μm; a minimum shift of 2.2 ± 1.4° is achieved by a current steering shift of 20 μm.

While investigating the EEP amplitude and the spatial spread for current steering, the electrode with the lowest threshold in a pair was set as E1 (α = 1; E2, α = 0) to eliminate differences between component electrodes among different electrode pairs. For each electrode pair, we calculated the averaged EEP amplitude (Amp_{avg}) of E1 and E2 alone (α = 1 and 0, Amp_1 and Amp_2, i.e., $Amp_{avg} = [Amp_1 + Amp_2]/2$), and the EEP amplitudes at each α were normalized with Amp_{avg}, that is, normalized EEP amplitude = actual EEP amplitude/Amp_{avg}. The same mathematic procedure was also done to HWHM in the spatial spread analysis when using current steering. The amplitude and spatial spread of the EEPs in response to different current coefficients are shown in Figures 9 and 10,

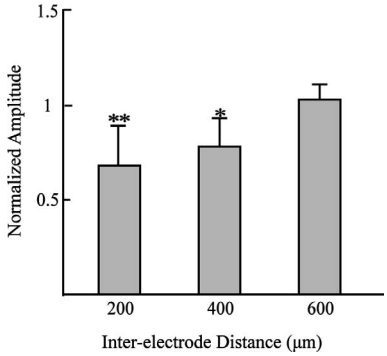

Figure 6. Comparison of EEP amplitudes using the single-electrode stimulation mode versus current steering mode. To eliminate individual differences between electrode pairs, data were normalized according to the following equation:

$$Amp_n = \frac{Amp_1 + Amp_2}{Amp_c} \quad (2)$$

where Amp_c is the EEP amplitude from each pair with current steering at I_t and an α of 0.5; Amp_1 and Amp_2 are the EEP amplitudes from separate single-electrode stimulation with E1 or E2 at $I_t/2$, and the Amp_n is the normalized summation amplitude of Amp_1 and Amp_2, which was expressed as the fraction of Amp_c; thus, $Amp_n < 1$ means the amplitude with current steering is larger than the summation of the independent amplitudes evoked by single-electrode stimulation of E1 and E2: 200 μm, $n = 8$ in five rabbits; 400 μm, $n = 4$ in two rabbits; 600 μm, $n = 2$ in one rabbit. $I_t = 1.5I_b$. $^{**}P < 0.01$; $^{*}P < 0.05$, paired t-test.

respectively. Changes in the α while maintaining the same total current resulted in EEP amplitudes and HWHMs that showed regular gradual shifts between that evoked by E1 or E2 alone (Figs. 9A–9C, 10A–C). Statistical analyses showed that there was no significant difference in the amplitudes or the spatial spread in response to single-electrode versus current steering stimulation at interelectrode distances of 200, 400, and 600 μm ($P > 0.05$ for both; Figs. 9D, 10D).

Simulation of ON Fiber Recruitment in Response to Steering Stimulation

Figure 11 summarizes the RA and SR for the current steering mode with different total currents I_t, steering coefficients α, and interelectrode distances. As illustrated in Figure 11, the RA increased with an increment in stimulating current intensity, whereas α and interelectrode distance had a very small impact on RA, especially at the lower current levels. The SR representing the recruitment centroid of ON fibers gradually shifted to the midpoint of two physical electrodes (SR = 0) as the α varied from 0.1 to 0.5, regardless of the variations of current intensity and interelectrode distance.

Discussion

Current steering is a widely applied field shaping strategy that uses the interaction between multiple electrodes to stimulate neural regions intermediate between the electrodes and thus augments the number of possible stimulation sites and improves spatial resolution. Our results clearly show that we could shift the spatial location of the cortical response by altering the simultaneous stimulation of closely spaced electrode pairs with currents that were lower than the thresholds of the component electrodes. The amplitudes and spatial spreads of the maximum evoked responses remained relatively stable as α was gradually changed at a fixed current intensity, showing no difference between the steering and single-electrode modes.

Current steering stimulation with α = 0.5, that is, simultaneous stimulation of E1 and E2 and evenly distributed currents, was used to compare the threshold and amplitude with single-electrode stimulation. Results demonstrated that with interelectrode distances of 200 and 400 μm, cortical EEPs could be evoked with a minimum current level that was lower than the single-electrode thresholds. Threshold reductions are commonly seen with simultaneous stimulation in cochlear implants and retinal stimulation.[41–44] In an animal study using penetrating auditory nerve electrodes and recording from the inferior colliculus, Middelebrooks et al.[43] reported threshold

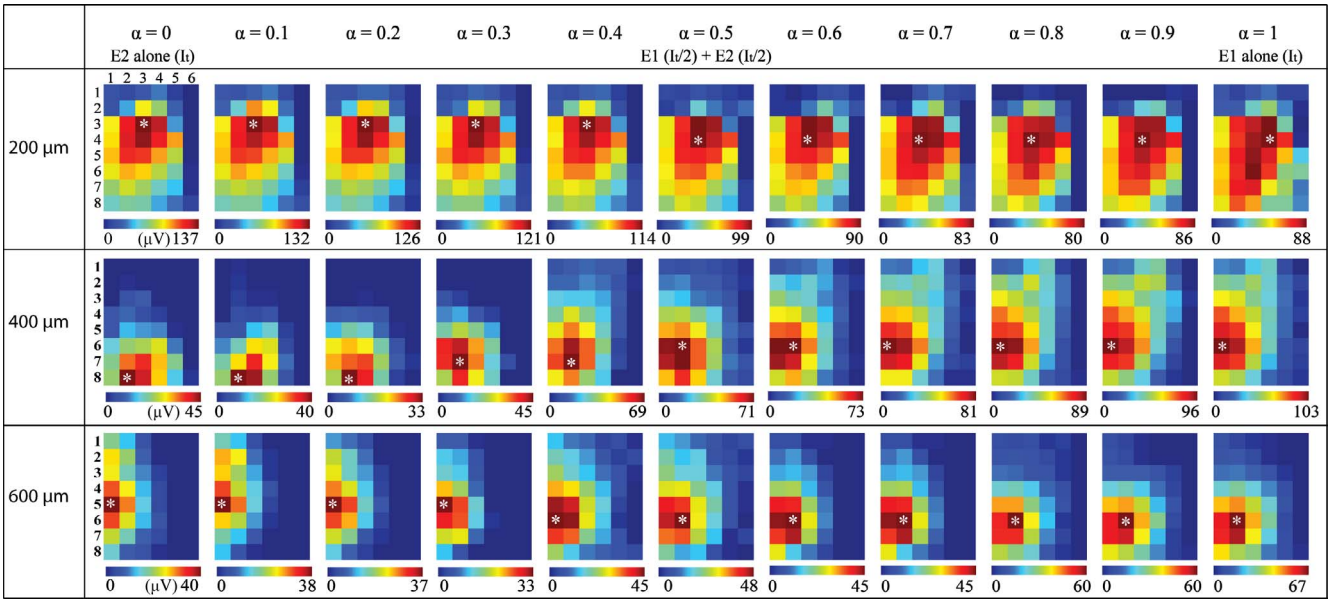

Figure 7. Distribution of cortical EEP amplitude following ON stimulation using various steering coefficients (α) and different interelectrode distances. *Asterisks* mark the EEP HChs. Note the gradual shift in the spatial distribution as α changes in 0.1 steps. $I_t = 1.5I_b$; data were recorded from three animals: 200 μm, rabbit 03; 400 μm, rabbit 06; 600 μm, rabbit 08.

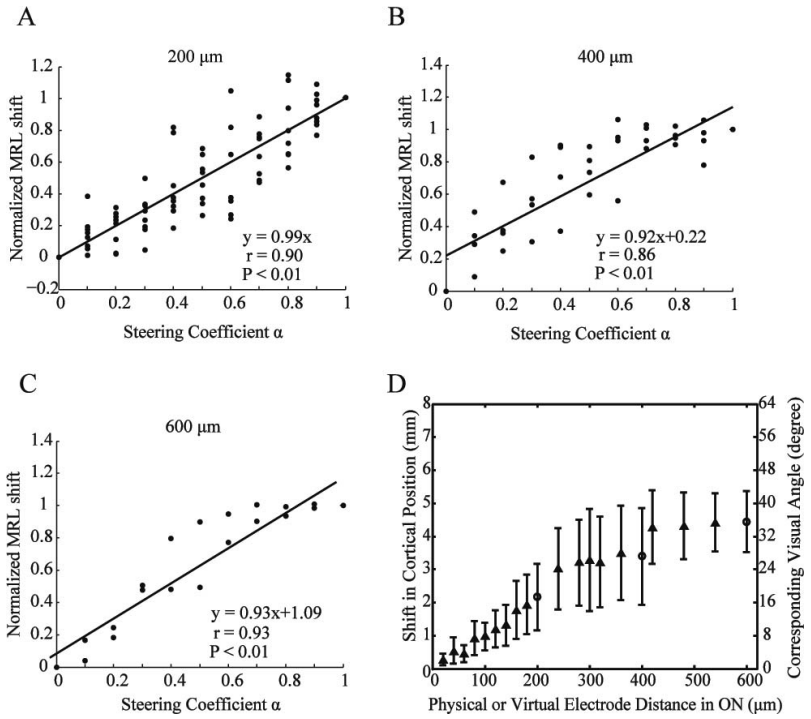

Figure 8. Shifts in the position of the relative cortical MRL to ON stimulation using various steering coefficients (α) and different interelectrode distances. (**A–C**) Linear regression analysis between normalized MRL shifts and steering coefficient. The *solid line* represents the fitted function. (**D**) Corresponding shift in cortical position and the converted visual angles for actual interelectrode distances in ON (*circles*) and the virtual interelectrode distances (*triangles*) created by different steering coefficients. $I_t = 1.5I_b$; 200 μm, $n = 8$ pairs in five rabbits; 400 μm, $n = 4$ in two rabbits; 600 μm, $n = 2$ in one rabbit.

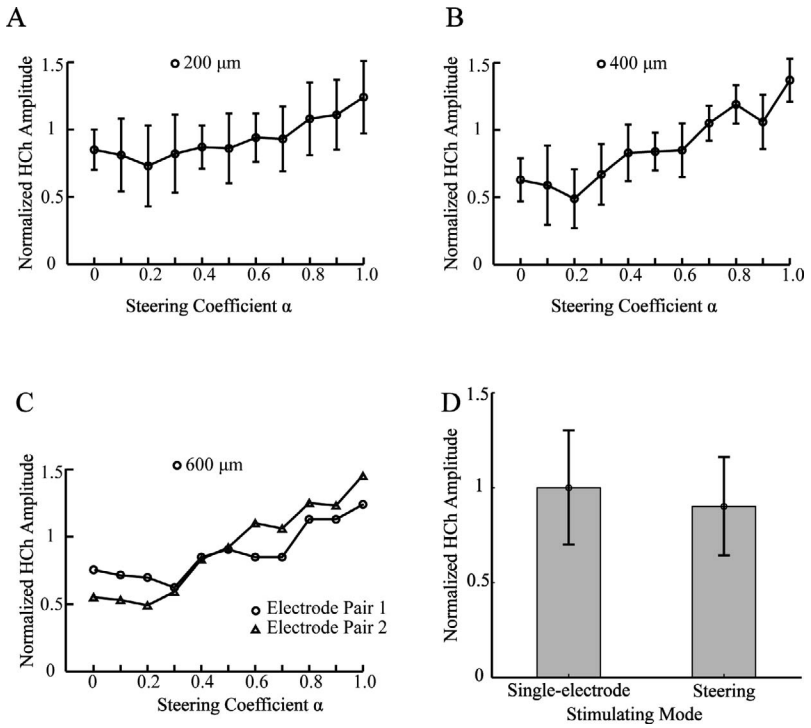

Figure 9. Cortical EEP amplitude changes in response to ON stimulation with various steering coefficients (α) and different interelectrode distances. The EEP amplitudes with $\alpha = 0$ and $\alpha = 1$ were averaged and set to 1, and amplitudes were normalized with it. (**A–C**) Amplitude changes and interelectrode distances. $I_t = 1.5I_b$, 200 μm, $n = 8$ pairs in five rabbits; 400 μm, $n = 4$ in two rabbits; 600 μm, $n = 2$ in one rabbit. (**D**) The recorded amplitudes during steering ($\alpha = 0.1 \sim 0.9$) and single-electrode modes ($\alpha = 0$ or 1) were not significantly different. Single-electrode: $n = 28$ pairs, eight rabbits; steering mode: $n = 126$; interelectrode distance data were combined from all experiments.

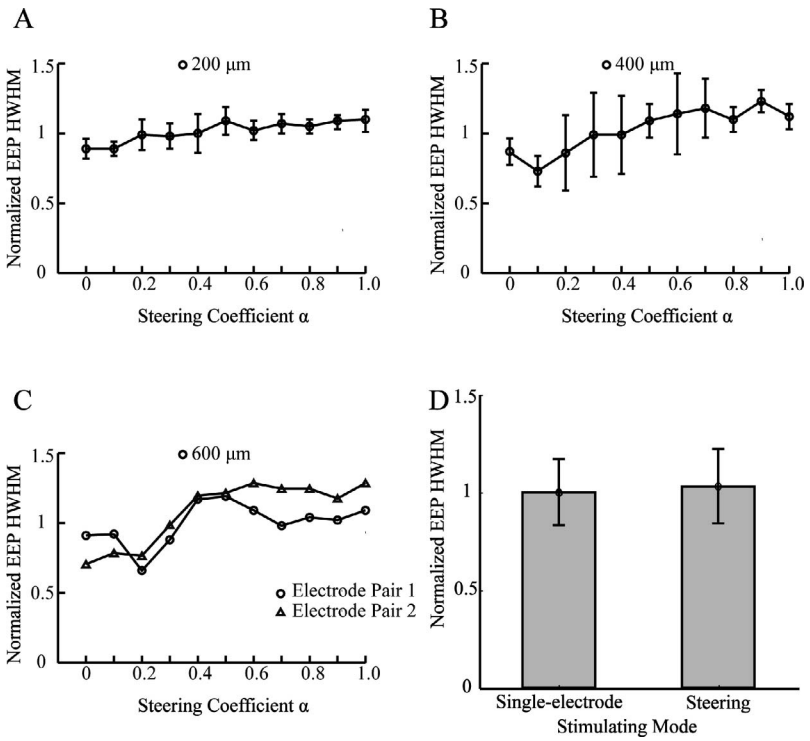

Figure 10. Spatial spread of the cortical EEPs using various steering coefficients (α) and different inter-electrode distances. The EEP HWHMs with $\alpha = 0$ and $\alpha = 1$ were averaged and set to 1, and HWHMs were normalized with it. (**A**–**C**) Spatial spread changes and inter-electrode distances. $I_t = 1.5I_b$, 200 μm, $n = 8$ pairs in five rabbits; 400 μm, $n = 4$ in two rabbits; 600 μm, $n = 2$ in one rabbit. (**D**) The normalized EEP HWHMs during steering ($\alpha = 0.1 \sim 0.9$) and single-electrode modes ($\alpha = 0$ or 1) were not significantly different. Single-electrode: $n = 28$ pairs, eight rabbits; steering mode: $n = 126$; interelectrode distance data were combined from all experiments.

reductions with interelectrode spacing of 200–600 μm, similar to our results. Consistent with the threshold reduction, EEP amplitudes with current steering and a current strength of I_t were higher than the summation of the independent E1 and E2 amplitudes at a current strength of $I_t/2$. The lower thresholds are believed to reflect an interaction between adjacent electrodes.[45,46] The EEP enhancement also indicates that it is not simply due to amplitude summation of the component electrodes, but due to increased fiber recruitment in the ON due to the overlapping electric fields and neural interactions that in turn lead to an augmented cortical response or recruitment of more extensive cortical networks within V1.[42,46–49] The changes in the cortical threshold were a conservative estimate of the ON interactions as it only revealed the effect at threshold, that is, the lowest current strength level. It cannot exclude the possibility of further interactions at higher current levels, given that the electric field in the ON and the cortical activation area are likely to increase.

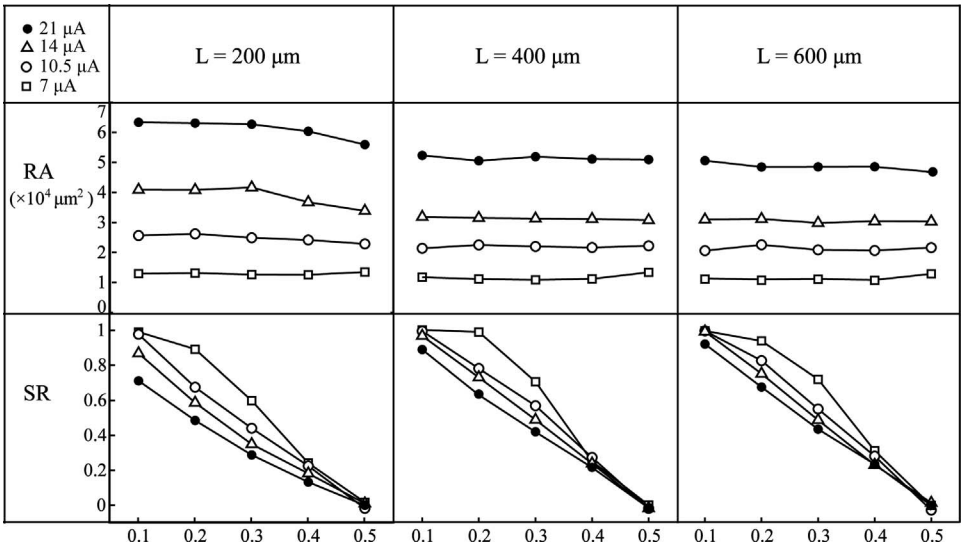

Figure 11. Simulation of ON fiber recruitment in response to steering stimulation. The RA and SR of paired stimulating electrodes using different total current I_t , steering coefficient α, and interelectrode distances.

Our results demonstrate that as current intensity gradually changes from one electrode to the other there is a linear shift in the location of the peak cortical response between the responses evoked by the component electrodes. These results imply that the visuotopic focus of the cortical response is shifted with current steering, and thus, it is possible to create multiple cortical representations in addition to those created by single electrode stimulation. This creates the possibility of increasing the spatial resolution of prosthesis through these virtual electrode (stimulation) sites. In both single and steering modes, larger ON interelectrode distances resulted in larger shifts in the position of the peak cortical response. A ~17° shift in the site of cortical activity could be seen with an interelectrode distance of 200 μm, whereas current steering at this interelectrode distance and a 0.1 α step, achieved a much smaller cortical shift of ~2.2° with a virtual electrode shift of 20 μm. Although these results are applicable only to the rabbit, they do suggest that even finer spatial shifts may be possible with human ON implants due to the higher density of foveal fibers and the increased cortical magnification factor in humans.[50,51] However, whether these spatial shifts of MRL could lead to changes in the visual percept should be confirmed in additional animal and, ultimately, human studies. Further studies in nonhuman primates will provide information about the possibilities of increasing prosthetic resolution using current steering at different interelectrode distances in the ON.

Visuotopic correspondence of the electrical stimulation to a retinotopic map is an important issue for visual restoration. Histologic studies have showed that there is only a rough retinotopic arrangement of retinal ganglion cell (RGC) fibers at the ON head, and these fibers gradually scattered and degrade the topographic map with the increasing distance from the eyeball.[52,53] We have implanted the stimulating electrodes ~1–2 mm behind the eyeball, and Lu et al.[32] showed that electrical stimulation at multiple sites and different depths at this location can result in the stimulation of a rough visuotopic map within the cortex. Relatively regular spatial shifts were observed in present study. However, due to the compaction of the RGC fibers from the entire retina into the small area of the ON, component electrodes with large interelectrode distances or stimulating with high current strengths will decrease the likelihood of creating a continuous retinotopic map and may generate nonadjacent phosphenes when using current steering.

The EEP threshold reduction and amplitude enhancement were only observed in current steering with interelectrode distances of 200 and 400 μm, but not 600 μm. However, spatial shifts in the cortical activity were found in steering stimulation at all three interelectrode distances. Thresholds, amplitudes, and spatial shifts of the cortical activity were relatively independent indices that describe different aspects of the electric field interaction. The former two are more likely to be related to the number of recruited ON fibers involved in the generation of the cortical response, whereas a spatial shift reflects the variation in the activated cortical areas. The spatial distribution of cortical responses could vary even if the total activated area did not change, whereas the cortical activated area is thought to be closely related to the recruited ON fiber number. Our results suggest that the interelectrode distance may have a different impact on the electric field interaction in steering stimulation.

When the total current strength was kept fixed during ON current steering, the spatial spread and amplitude of the cortical responses remained relatively stable, and there were no significant differences between current steering ($\alpha = 0.1\sim0.9$) and single-electrode modes ($\alpha = 0$ or 1). For each α, Dumm et al.[37] analyzed spatial selectivity across all cortical recording electrodes at a current level required to reach 90% of maximum cortical response on the best cortical electrode (cortical electrode with the lowest threshold) and thus measured selectivity at the same point on the electrical dynamic range for each α. They saw no differences in cortical selectivity between physical electrodes ($\alpha = 0$ or 1) and virtual electrodes ($\alpha = 0.1\sim0.9$) in their study of current steering in suprachoroidal retinal stimulation. In the computer modeling studies on current steering of cochlear implants by Frijins et al.,[54] the spatial width of the excited region also remained stable with varied α as the stimulus currents were applied relative to the most comfortable level (MCL) of the respective electrodes. Although similar phenomena have been observed in these studies, the stimulation conditions were different. Our results revealed the response properties using a fixed current strength without matching the stimulating levels with respect to the thresholds at varied α. It is a very important issue to measure the threshold at each α during current steering and compare the evoked responses using stimulus currents based on the specific α thresholds to keep the stimulation at the same region of dynamic range for both steering and single-electrode modes. This investigation needs to be explored further in a future study to acquire a more comprehensive understanding of current steering for the penetrating ON prosthesis.

Finally, we established computational models to evaluate the effects of current steering on ON fibers. The simulation results show that the SR changes with the steering coefficient; this revealed that the distributions of electric fields and recruited ON fibers could be spatially modulated by current steering, which is a necessary condition for generating virtual electrodes within the ON. However, when current intensity is fixed, the RA is basically stable with different steering coefficients, indicating that the number of the ON fibers involved did not change to any considerable degree and is consistent with our electrophysiological results in which the cortical response amplitude and spatial spread remained stable with steering stimulation. The RA and SR only reflected the effect of current steering on the ON fibers; however, whether this influence will be changed and to what extent it will be changed during the information processing of the downstream neural network, that is, the lateral geniculate nucleus and visual cortex, remains unknown. Therefore, our simulation results can only be interpreted as a limited and conservative estimation of the effect of current steering in the ON, and this should be considered when comparing these results with the cortical responses.

In summary, our electrophysiological and simulated results confirm the viability of using closely spaced penetrating ON electrodes and current steering to alter the visuotopic focus of evoked cortical responses. A penetrating ON prosthesis has merit due to its potential to elicit cortical responses within a large area of the visual field. However, the limited number of electrodes within a possible array constrains visual resolution; thus, current steering may prove to be a very efficient tool to improve spatial resolution. Only a linear arrangement of electrode pairs was investigated in this study as a first step in exploring the feasibility and basic characteristics of current steering for a penetrating ON prosthesis. However, ON anatomy makes it possible to implant a more complex 3D pattern of electrodes, for example, incorporating different depths within the ON. Our future studies will investigate current steering with this multidimensional arrangement in our quest to further improve the virtual spatial resolution of a prosthetic device.

Acknowledgments

The authors thank Thomas FitzGibbon for comments on previous drafts of the manuscript.

Supported by the National Basic Research Program of China (973 Program, 2011CB707502) and the National Natural Science Foundation of China (61671300, 61171174, 60971102, 91120304, 61472247).

Disclosure: **Y. Yan**, None; **Y. Lu**, None; **M. Li**, None; **Z. Ma**, None; **P. Cao**, None; **Y. Chen**, None; **X. Sun**, None; **X. Chai**, None; **Q. Ren**, None; **L. Li**, None

References

1. Humayun MS, Dorn JD, da Cruz L, et al. Interim results from the international trial of Second Sight's visual prosthesis. *Ophthalmology*. 2012;119:779–788.
2. Rizzo JF III. Update on retinal prosthetic research: the Boston Retinal Implant Project. *J Neuroophthalmol*. 2011;31:160–168.
3. Menzel-Severing J, Laube T, Brockmann C, et al. Implantation and explantation of an active epiretinal visual prosthesis: 2-year follow-up data from the EPIRET3 prospective clinical trial. *Eye (Lond)*. 2012;26:501–509.
4. Fujikado T, Morimoto T, Kanda H, et al. Evaluation of phosphenes elicited by extraocular stimulation in normals and by suprachoroidal-transretinal stimulation in patients with retinitis pigmentosa. *Graefes Arch Clin Exp Ophthalmol*. 2007;245:1411–1419.
5. Veraart C, Raftopoulos C, Mortimer JT, et al. Visual sensations produced by optic nerve stimulation using an implanted self-sizing spiral cuff electrode. *Brain Res*. 1998;813:181–186.
6. Dobelle WH, Mladejovsky MG. Phosphenes produced by electrical stimulation of human occipital cortex, and their application to the development of a prosthesis for the blind. *J Physiol*. 1974;243:553–576.
7. Pezaris JS, Reid RC. Demonstration of artificial visual percepts generated through thalamic microstimulation. *Proc Natl Acad Sci U S A*. 2007;104:7670–7675.
8. Zrenner E, Stett A, Weiss S, et al. Can subretinal microphotodiodes successfully replace degenerated photoreceptors? *Vision Res*. 1999;39:2555–2567.
9. Chuang AT, Margo CE, Greenberg PB. Retinal implants: a systematic review. *Br J Ophthalmol*. 2014;98:852–856.
10. Brindley GS, Lewin WS. The visual sensations produced by electrical stimulation of the medial occipital cortex. *J Physiol*. 1968;194:54P–55P.
11. Normann RA, Maynard EM, Rousche PJ, Warren DJ. A neural interface for a cortical vision prosthesis. *Vision Res*. 1999;39:2577–2587.
12. Chowdhury V, Morley JW, Coroneo MT. Evaluation of extraocular electrodes for a retinal prosthesis using evoked potentials in cat visual cortex. *J Clin Neurosci*. 2005;12:574–579.
13. Palanker D, Vankov A, Huie P, Baccus S. Design of a high-resolution optoelectronic retinal prosthesis. *J Neural Eng*. 2005;2:S105–S120.
14. Chai X, Li L, Wu K, Zhou C, Cao P, Ren Q. C-sight visual prostheses for the blind. *IEEE Eng Med Biol Mag*. 2008;27:20–28.
15. Zhou JA, Woo SJ, Park SI, et al. A suprachoroidal electrical retinal stimulator design for long-term animal experiments and in vivo assessment of its feasibility and biocompatibility in rabbits. *J Biomed Biotechnol*. 2008;2008:547428.
16. Villalobos J, Allen PJ, McCombe MF, et al. Development of a surgical approach for a wide-view suprachoroidal retinal prosthesis: evaluation of implantation trauma. *Graefes Arch Clin Exp Ophthalmol*. 2012;250:399–407.
17. Stingl K, Bartz-Schmidt KU, Besch D, et al. Artificial vision with wirelessly powered subretinal electronic implant alpha-IMS. *Proc Biol Sci*. 2013;280:20130077.
18. World Health Organization. Blindness and low vision. In: *International Statistical Classification of Diseases and Related Problem*. 10th revision, Chapter VII, H54.
19. Rizzo JF III, Wyatt J, Loewenstein J, Kelly S, Shire D. Perceptual efficacy of electrical stimulation of human retina with a microelectrode array during short-term surgical trials. *Invest Ophthalmol Vis Sci*. 2003;44:5362–5369.
20. Eckmiller R. Learning retina implants with epiretinal contacts. *Ophthalmic Res*. 1997;29:281–289.
21. Fried SI, Hsueh HA, Werblin FS. A method for generating precise temporal patterns of retinal spiking using prosthetic stimulation. *J Neurophysiol*. 2006;95:970–978.
22. Wilms M, Eger M, Schanze T, Eckhorn R. Visual resolution with epi-retinal electrical stimulation estimated from activation profiles in cat visual cortex. *Vis Neurosci*. 2003;20:543–555.
23. Chow AY, Chow VY, Packo KH, Pollack JS, Peyman GA, Schuchard R. The artificial silicon retina microchip for the treatment of vision loss from retinitis pigmentosa. *Arch Ophthalmol*. 2004;122:460–469.
24. Pardue MT, Ball SL, Phillips MJ, et al. Status of the feline retina 5 years after subretinal implantation. *J Rehabil Res Dev*. 2006;43:723–732.
25. Tsai D, Morley JW, Suaning GJ, Lovell NH. Direct activation and temporal response properties of rabbit retinal ganglion cells following subretinal stimulation. *J Neurophysiol*. 2009;102:2982–2993.
26. Villalobos J, Nayagam DA, Allen PJ, et al. A wide-field suprachoroidal retinal prosthesis is stable and well tolerated following chronic implantation. *Invest Ophthalmol Vis Sci*. 2013;54:3751–3762.
27. Cicione R, Shivdasani MN, Fallon JB, et al. Visual cortex responses to suprachoroidal electrical stimulation of the retina: effects of electrode return configuration. *J Neural Eng*. 2012;9:036009.
28. Fang X, Sakaguchi H, Fujikado T, et al. Electrophysiological and histological studies of chronically implanted intrapapillary microelectrodes in rabbit eyes. *Graefes Arch Clin Exp Ophthalmol*. 2006;244:364–375.
29. Veraart C, Wanet-Defalque MC, Gerard B, Vanlierde A, Delbeke J. Pattern recognition with the optic nerve visual prosthesis. *Artif Organs*. 2003;27:996–1004.
30. Li L, Cao P, Sun M, et al. Intraorbital optic nerve stimulation with penetrating electrodes: in vivo electrophysiology study in rabbits. *Graefes Arch Clin Exp Ophthalmol*. 2009;247:349–361.
31. Sun J, Lu Y, Cao P, et al. Spatiotemporal properties of multipeaked electrically evoked potentials elicited by penetrative optic nerve stimulation in rabbits. *Invest Ophthalmol Vis Sci*. 2011;52:146–154.
32. Lu Y, Yan Y, Chai X, Ren Q, Chen Y, Li L. Electrical stimulation with a penetrating optic nerve electrode array elicits visuotopic cortical responses in cats. *J Neural Eng*. 2013;10:036022.
33. Bonham BH, Litvak LM. Current focusing and steering: modeling, physiology and psychophysics. *Hear Res*. 2008;242:141–153.
34. Berenstein CK, Mens LH, Mulder JJ, Vanpoucke FJ. Current steering and current focusing in cochlear implants: comparison of monopolar, tripolar and virtual channel electrode configurations. *Ear Hear*. 2008;29:250–260.
35. Jepson LH, Hottowy P, Mathieson K, et al. Spatially patterned electrical stimulation to enhance resolution of retinal prostheses. *J Neurosci*. 2014;34:4871–4881.
36. Jepson LH, Hottowy P, Weiner GA, Dabrowski W, Litke AM, Chichilnisky EJ. High-fidelity reproduction of spatiotemporal visual signals for retinal prosthesis. *Neuron*. 2014;83:87–92.

37. Dumm G, Fallon JB, Williams CE, Shivdasani MN. Virtual electrodes by current steering in retinal prostheses. *Invest Ophthalmol Vis Sci*. 2014;55:8077–8085.
38. Choudhury BP. Visual cortex in the albino rabbit. *Exp Brain Res*. 1987;66:565–571.
39. Yan Y, Sui X, Liu W, et al. Spatial characteristics of evoked potentials elicited by a MEMS microelectrode array for suprachoroidal-transretinal stimulation in a rabbit. *Graefes Arch Clin Exp Ophthalmol*. 2015;253:1515–1528.
40. Li M, Yan Y, Wang Q, et al. A simulation of current focusing and steering with penetrating optic nerve electrodes. *J Neural Eng*. 2013;10:066007.
41. Middlebrooks JC. Effects of cochlear-implant pulse rate and inter-channel timing on channel interactions and thresholds. *J Acoust Soc Am*. 2004;116:452–468.
42. Bierer JA, Middlebrooks JC. Cortical responses to cochlear implant stimulation: channel interactions. *J Assoc Res Otolaryngol*. 2004;5:32–48.
43. Middlebrooks JC, Snyder RL. Auditory prosthesis with a penetrating nerve array. *J Assoc Res Otolaryngol*. 2007;8:258–279.
44. Shivdasani MN, Luu CD, Cicione R, et al. Evaluation of stimulus parameters and electrode geometry for an effective suprachoroidal retinal prosthesis. *J Neural Eng*. 2010;7:036008.
45. Townshend B, White RL. Reduction of electrical interaction in auditory prostheses. *IEEE Trans Biomed Eng*. 1987;34:891–897.
46. Stickney GS, Loizou PC, Mishra LN, Assmann PF, Shannon RV, Opie JM. Effects of electrode design and configuration on channel interactions. *Hear Res*. 2006;211:33–45.
47. Horsager A, Greenberg RJ, Fine I. Spatiotemporal interactions in retinal prosthesis subjects. *Invest Ophthalmol Vis Sci*. 2010;51:1223–1233.
48. Horsager A, Boynton GM, Greenberg RJ, Fine I. Temporal interactions during paired-electrode stimulation in two retinal prosthesis subjects. *Invest Ophthalmol Vis Sci*. 2011;52:549–557.
49. de Balthasar C, Boex C, Cosendai G, Valentini G, Sigrist A, Pelizzone M. Channel interactions with high-rate biphasic electrical stimulation in cochlear implant subjects. *Hear Res*. 2003;182:77–87.
50. Cowey A, Rolls ET. Human cortical magnification factor and its relation to visual acuity. *Exp Brain Res*. 1974;21:447–454.
51. Curcio CA, Allen KA. Topography of ganglion cells in human retina. *J Comp Neurol*. 1990;300:5–25.
52. Fitzgibbon T, Taylor SF. Retinotopy of the human retinal nerve fibre layer and optic nerve head. *J Comp Neurol*. 1996;375:238–251.
53. Naito J. Course of retinogeniculate projection fibers in the cat optic nerve. *J Comp Neurol*. 1986;251:376–387.
54. Frijns JH, Kalkman RK, Vanpoucke FJ, Bongers JS, Briaire JJ. Simultaneous and non-simultaneous dual electrode stimulation in cochlear implants: evidence for two neural response modalities. *Acta Otolaryngol*. 2009;129:433–439.

Investigative Ophthalmology & Visual Science